Realization of Omnidirectional CubeSat Crosslink by Wavelength-Selective Optical Transceiver

Imam Uz Zaman[ID], Jose E. Velazco, and Ozdal Boyraz[ID]

Abstract—**Advanced space missions, e.g., interplanetary exploration and Earth observation embrace constellation or swarm-like CubeSat configuration to achieve unprecedented spatial and temporal resolutions at a significantly lower investment. The realization of high-speed inter-CubeSat data communication link is mandatory to ensure the success of such missions. In this article, we present a scalable high-speed CubeSat crosslink implementation based on the wavelength-selective optical transceiver (WSOT) design. System performance based on the state-of-the-art components that satisfy the stringent size, weight, power, and cost requirements has been investigated. We estimate that with a 15 mm transceiver aperture size and 1 W peak bit power, the system attains communication distance up to 125 and 80 km for 400 Mb/s and 800 Mb/s data rates, respectively. Additionally, we present the optical and mechanical design of five transceiver units that can fit inside a 3U CubeSat to achieve a full field of regard (360°) to enable omnidirectional high-speed optical communication. Further performance improvements are possible through incorporating advanced amplifiers, error correction coding, and large aperture optics.**

Index Terms—**CubeSat crosslink, free-space optical link, omnidirectional optical antenna, optical transceiver, satellite communication.**

I. Introduction

CUBESAT technology (a class of nanosatellites) continues to evolve to tackle more advanced and challenging space missions. An engineered CubeSat constellation (multiple CubeSat performing time-synchronized operations) as shown in Fig. 1 can offer an unprecedented massive spaceborne system to pave the way to new applications that are not conventionally attainable. Size, weight, power, and cost (SWaP-C)

has never become so important as it is in CubeSat where performance metrics clash with available size and power. Small, affordable, and transformative approaches that comply with the extreme SWAP-C constraints and enable high-speed data communication, as well as autonomous navigation, are indispensable to attain a comparable performance metrics of those of large systems [1]. In particular, 3-D constellations in space require omnidirectional data communicators that can establish point-to-point data communications and also data relaying among an arbitrary set of CubeSats or major satellites. Modern wireless intersatellite communications are mostly based on microwave technologies [2]–[4]. However, the lack of sufficient power and the permissible antenna size limit the performance of the conventional microwave communication technologies in CubeSats. The optical transceivers, on the other hand, provide a compact architecture and a larger antenna gain that can enhance the data rate over the microwave counterparts. Up to date, several optical communication methods have been explored for minisatellite and microsatellite [5]–[7]. Among many of these methods, most of the efforts have been given on the long-range low-Earth orbit (LEO) to Earth point-to-point data communications which utilize large ground telescopes (in the order of meters in dimension) as the receiver terminal. For instance, LEO to Earth optical communication with a data rate as high as 1 Gb/s is demonstrated in small satellite platforms (up to 6.0 kg payload incorporated in a 130 kg satellite that produces up to 1 W optical transmit power with about 37 W electrical power consumption [6], [7]). Kaufmann and Chan [4] analyzed the feasibility of a coherent system that can fit in a small satellite platform in an effort to address the power and size constraints imposed by small satellite platforms. The analyses show up to 100 Mb/s point-to-point laser communication with a 20 cm aperture and 30 mW laser source.

The optical communication between CubeSats with more stringent SWaP-C limits is a relatively new area of research and development. LED array-based LEO to Earth communication at 5 kHz with 200 W peak optical power is achieved in an experimental CubeSat (FITSAT-1) as one of the earlier developments in this field [8]. Similarly, LEO to Earth communication with 100 Mb/s data rate and up to 20 W electrical power consumption has been demonstrated in [9]
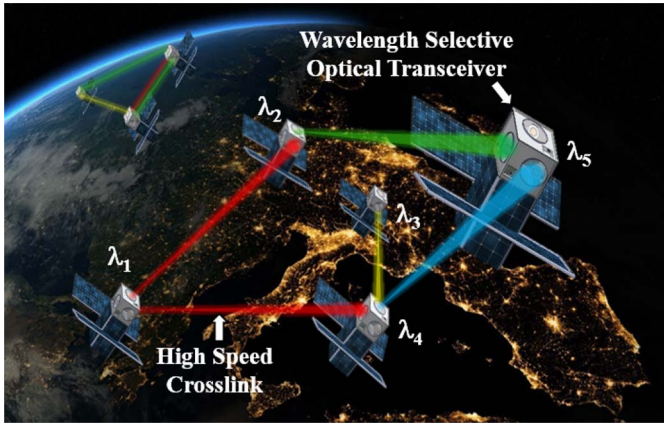
Fig. 1. Inter-CubeSat data communication using WSOT.

Fig. 2. Omnidirectional transceiver architectures. (a) Incorporated with high-speed MEMS mirrors. (b) Incorporated with large diameter DAV mirrors.

and [10]. A current NASA mission (CubeSat crosslink mission, CLICK) sets a goal to achieve 20 Mb/s at ranges from 25 to 580 km by incorporating a 500 mW laser [11]. To the best of our knowledge, all the research and development work on the satellite optical links (LEO–LEO and LEO–Earth) have been done either for satellites with significantly less SWaP-C constraints or for a single point-to-point (one-to-one) data communication link. However, constellation and formation fly of such satellites necessitate optical communicator with omnidirectionality and data relaying capabilities to minimize data storage (DS) and onboard electronic processing [12]–[14]. Omnidirectional (one-to-many) high-speed data communication and data relaying capability among small satellites are still open for investigation in the optical domain.

This article presents an optical communicator design based on a CubeSat scale wavelength-selective optical transceiver (WSOT) system architecture that can achieve a 360° field of regard (FOR), longer than 100 km communication distance, and more than 400 Mb/s data rates. Our analyses utilize the Zemax-based optical telescope design, experimental studies on the FlatSat model followed by numerical validation of the achievable communication range and power consumption. A conservative bit error rate (BER) estimation based on the Gaussian statistical analysis [15] is also performed on the received signal. We experimentally show that in the worst case scenario (in the absence of advanced transimpedance amplifier (TIA), error correction coding, etc.), the achievable receiver sensitivities are -33 dBm and -28.5 dBm at 200 and 400 MHz, respectively, to generate BER is less than or equal to 10^{-4}. Considering the receiver sensitivity, we estimate that with a 1-W peak transmit power (500-mW average power with 50% duty cycle) and 15 mm transceiver aperture (TA), the WSOT system can achieve communication distances up to 125 and 80 km for 400 Mb/s and 800 Mb/s nonreturn-to-zero (NRZ) signals, respectively. We also discuss how to scale the system performance in terms of power and maximum reach.

II. Omnidirectional Antenna Design and the Transceiver Architecture

A wide FOR optical transmitter is a must to implement a long-range omnidirectional data communicator. The gain G_T of the optical transmitter can be increased by increasing the ratio of transmitter beam size D_T to the operating wavelength λ and can be expressed as $G_T \approx (\pi D_T/\lambda)^2$. The wide FOR can be realized in the transmitter architecture by incorporating a fast beam scanning mechanism, e.g., scanning mirrors and phased array antenna. The required number of transmitters n_T can be estimated from the steering range α_s of the scanning mechanism and the required FOR (full angle) α_{rec} and can be expressed as
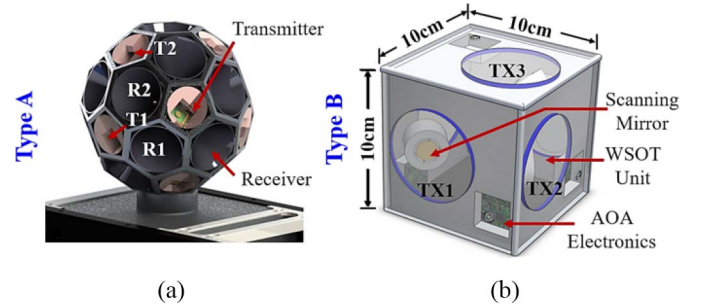
$$n_T \approx \mathrm{ceiling}\left(\left(\frac{\sin(\pi\alpha_{\mathrm{req}}/720)}{\sin(\pi\alpha_s/360)}\right)^2\right).$$

If a scanning mirror is used for the scanning purpose, the mechanical scanning angle α_{mec} of the mirror can be defined as $\alpha_{\mathrm{mec}} = (1/2)\,\alpha_s$. Using the equation, one can find that 15, 9, and 6 independent transmitter branches are required to achieve a full field of view (360°) by incorporating a scanning mirror with 30°, 40°, and 50° full mechanical scanning ranges, respectively. Two of the most promising commercial-off-the-shelf (COTS) scanning mirror technologies that can achieve wide FOR and high-speed scanning are MEMS mirror [16] and dual-axis vector (DAV) scanning mirror [17]. These scanning mirrors possess tradeoffs among the size, the scanning speed, and the scanning angle. MEMS mirrors have a smaller diameter (less than 5 mm), small scanning angle (less than $\pm7°$) but high scanning frequency (more than 1 kHz). In contrast, DAV mirrors are generally large in diameter (greater than 10 mm). They have a high scanning angle (greater than 25°) but low scanning speed (smaller than 400 Hz). Based on these two different mirror mechanisms, two simple design approaches can be adopted to achieve omnidirectional optical antenna: 1) type A and 2) type B (as shown in Fig. 2). The type A approach incorporates MEMS mirrors. This type A design approach requires the independent transmitter and receiver apertures due to small transmit aperture (mirror) size. On the contrary, the type B design incorporates relatively larger DAV mirrors, and therefore, it allows using the same aperture to transmit and receive signals as shown in Fig. 2(b).

In addition to wide FOR transmitter, the receiver of the omnidirectional communicator must have high bandwidth, large aperture, and wide FOR simultaneously. The required average optical power P_{rec} is calculated from the required signal-to-noise ratio (SNR) $\mathrm{SNR}_{\mathrm{req}}$, total noise power of the receiver σ^2, photodiode gain M, and photodiode responsivity
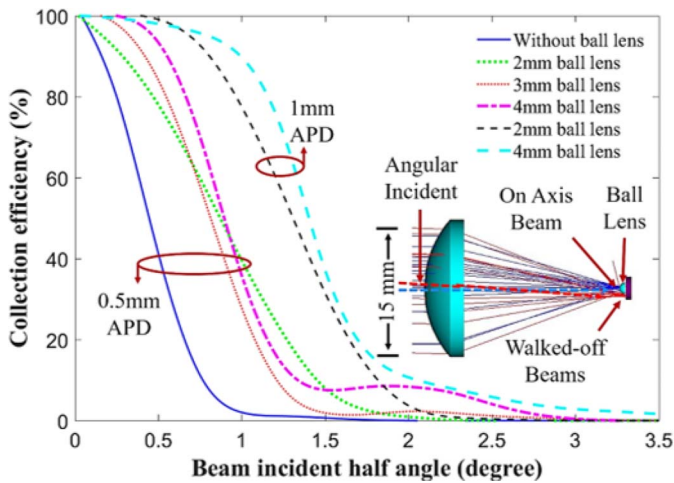
Fig. 3. FOV of sample direct detection receiver.

R_p, and can be given as $P_{\text{req}} \geq \sqrt{(\text{SNR}_{\text{req}} \sigma^2)/(R_P^2 M^2)}$. The receiver design should also consider the tradeoffs among the field of view (FOV), detector bandwidth, and power collection capability of the receiver optics. Omnidirectional receiver designs can be in an imaging optics-based receiver (IOR) architecture or nonimaging optics-based receiver (NOR) architecture. NORs are highly used in solar cells which possess tradeoffs among optical power collection efficiency, aperture size, volume, and achievable FOV. Besides, the NOR architecture requires a large optical path to accommodate a wide FOV that is not feasible in the CubeSat scale receiver design [18]–[20]. The FOV Ω_{FOV} of the simplest IOR design (as shown in Fig. 3) incorporating an aspheric lens (AL) along with an avalanche photodiode (APD) depends on the diameter of the detector H and the focal length of the focusing lens (FL) f: $\Omega_{\text{FOV}} \approx 2 \tan^{-1}(H/2f)$. It is desirable to use a large H to design a wide FOV receiver system. However, H is inversely proportional to bandwidth B, and hence, the wide FOV IOR receiver design has tradeoffs between detector size and bandwidth. In fact, the diameter of the available COTS high bandwidth APD (greater than 600 MHz) is less than 1.0 mm.

One effective way to increase the FOV of the detector is to incorporate a ball lens at the focal plane of the receiver lens as shown in Fig. 3 (inset). For example, in the absence of a ball lens, a detector system incorporating a 0.5 mm photodetector and a receiver lens of 15 mm diameter with a 30 mm focal length can achieve $\Omega_{\text{FOV}} = \pm 0.45°$ (efficiency $\geq 50\%$). However, we estimate that the FOV can be doubled ($\Omega_{\text{FOV}} \approx \pm 0.9°$) by using a half-ball lens of 4-mm (diameter). Furthermore, FOV improvement can be achieved by using larger detectors. For instance, incorporating a 1 mm detector along with a 2 mm half-ball lens can increase the FOV to $\pm 1.4°$ as shown in Fig. 3. Given a geometry and a predefined number of transmitters and receivers, the required FOV of the individual receiver in the type A architecture is in the range of 20°–65° to achieve omnidirectional optical signal collection. Hence, it is extremely challenging to satisfy both the FOV requirement and the large aperture requirement

by conventional the NOR and IOR designs. Complex optical system designs, such as focal plane detector array and fish-eye lens can achieve a wide FOV but mandates larger volume, complex electronics, and less effective aperture size [21].

An alternative approach to circumvent the wide FOV receiver design complexities is to employ a type B transceiver design approach as shown in Fig. 2(b). The main advantage of the type B transceiver design is that it can use the same aperture to both send and receive signals. As a result, due to the reciprocity of the optical beam propagation, once the communication link is set up, the type B design approach ensures a direct line-of-sight communication among communication nodes. For this reason, the type B transceiver design approach is a solution to evade the design difficulties pertinent to the omnidirectional communication systems described above.

III. WAVELENGTH-SELECTIVE OPTICAL TRANSCEIVER MODEL

Considering the design complexity of the multiaperture transceiver system design and the detector FOV requirement, we move forward with the WSOT-based constellation scheme that utilizes the type B transceiver architecture as illustrated in Fig. 2. In the WSOT-based CubeSat crosslink scheme, each CubeSat C_i in a constellation of n CubeSats is assigned to a unique wavelength (λ_i), where $i \in [1, n]$ as shown in Fig. 4. Each WSOT transceiver of the CubeSat C_i incorporates a unique dichroic filter (DF) with a center wavelength around λ_i and transmission bandwidth $\Delta\lambda$ so that the center wavelength $\lambda_c \approx \lambda_i$ and $\Delta\lambda < |\lambda_i - \lambda_{j=i\pm 1}| \, \forall i, j = 1, 2, 3, \ldots, n$. As a result, C_i transmits signals with λ_i to other CubeSats $C_{j\neq i}$ but it can detect all other wavelengths, $\lambda \neq \lambda_i$. For instance, in Fig. 4, CubeSat C_1 transmits λ_i to both C_4 and C_3. However, C_1 can detect signals of both wavelengths λ_2 and λ_4 from C_2 and C_4, respectively. The major implementation challenges in the WSOT system-based constellations are the data packet collision, the unique wavelength allocation to each CubeSat, and the fabrication of narrow bandwidth DFs. The possibility of packet collision occurs in the WSOT system when two or more transmitters are in the receiver's FOV and the received signal strengths are comparable. In other words, packet collision occurs if the angular separation between two transmitters (Ω_{TX}) with respect to the receiver is less than or equal to the full FOV of the receiver, $\Omega_{TX} \leq \Omega_{\text{FOV}}$. A collision detection protocol needs to be implemented in the media access control (MAC) layer of the network to overcome such problems as done in current Ethernet networks. The state-of-the-art ITU grids are being set at 100 GHz (about 0.8 nm) channel spacing at C and L bands, and hence more than 100 wavelength channels (i.e., more than 100 satellites) can be supported. The main implementation bottleneck at the time of writing this article is the lack of available COTS narrow bandwidth DFs. Even though only a few discrete wavelength dichroic bandpass filters are commercially available, custom fabricated filters for specific wavelengths can be attained from different manufacturers.

The transmitter (TX) of the WSOT system design as given in Fig. 5 incorporates a laser diode (L), an AL based
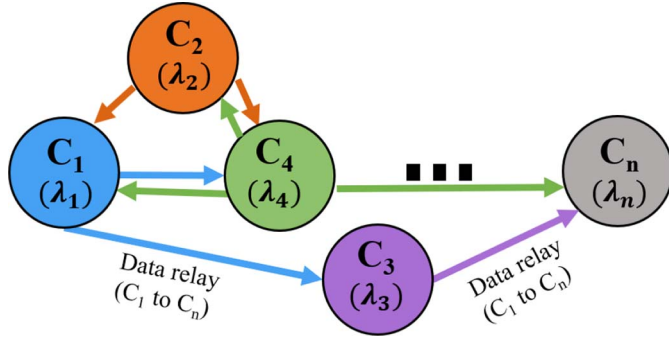
Fig. 4. WSOT-based CubeSat constellation concept.
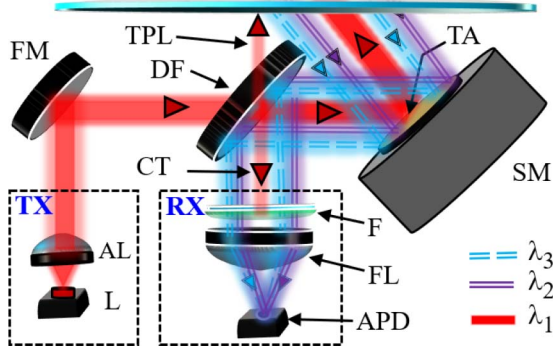
Fig. 5. WSOT optical architecture.

collimation system. A fixed mirror (FM) is used to make the TX chain compact to fit inside the CubeSat platform. A DF is integrated to enable wavelength-selective communication and to minimize the crosstalk. The receiver chain (RX) consists of a wideband filter (F), FL, and an APD as shown in Fig. 5. A steering mirror (SM) of diameter $2a$-based TA ensures a line-of-sight communication that facilitates the pointing and tracking mechanism.

The received optical power $P_{\mathrm{rcv}}(\lambda_i)$ can be estimated from the transmit power $P(\lambda_i)$, transmitter feeder loss $\alpha_{Ti}(\lambda_i)$, receiver chain loss $\alpha_{Rj}(\lambda_i)$, geometric loss $G(\lambda_i)$, pointing loss α_p, and atmospheric attenuation $\gamma(R)$ as $P_{\mathrm{rcv}}(\lambda_i) = P(\lambda_i)\alpha_{Ti}(\lambda_i)\alpha_{Rj}(\lambda_i)G(\lambda_i)\alpha_p\gamma(R)$. The total power of the optical beam with wavelength λ_i at the collimator's output can be calculated from the complex transverse electric field of the optical beam $E_c(r, z, \lambda_i)$ as $P(\lambda_i) = \iint |E_c(r, z, \lambda_i)|^2 dA$. Therefore, the transverse intensity profile of the beam at a distance z is represented by $I(r, z) = ([2P(\lambda_i)]/[\pi \cdot \omega(z)^2]) \exp([-2r^2]/[\omega(z)^2])$. Here, r is the radial distance away from the optical axis, $\omega_\circ$ is the transmit beam waist (radius), and $\omega(z)$ is the beam radius $(1/e^2)$ at a distance z. Assuming the optical length (l_{opt}) inside the WSOT transceiver is much smaller than the Rayleigh range, the intensity of the transmitted beam with wavelength λ_i at the WSOT transceiver output of CubeSat C_i can be approximated as $I_T(r, z = l_{\mathrm{opt}}) \approx ([2\alpha_{Ti}(\lambda_i)P(\lambda_i)]/[\pi\omega_\circ^2]) \exp([-2r^2]/[\omega_\circ^2])$. Here, $\alpha_{Ti}(\lambda_i)$ is the transmitter feeder loss that is a function of wavelength λ_i, the number of FMs n_{FM}, the reflectance of the mirrors $R_{\mathrm{FM}}(\lambda_i)$, the transmission of the DF $T_{\mathrm{DF}}(\lambda_i)$, the scanning mirror aperture radius a, and the reflectance

of the scanning mirror $R_{\mathrm{SM}}(\lambda_i)$. $\alpha_{Ti}(\lambda_i)$ can be given as $\alpha_{Ti}(\lambda_i) = n_{\mathrm{FM}}R_{\mathrm{FM}}(\lambda_i)R_{\mathrm{SM}}(\lambda_i)T_{\mathrm{DF}}(\lambda_i)(1-\exp([-2a^2]/[\omega_\circ^2]))$.

The beam experiences pointing loss α_p, attenuation $\gamma(R) = \exp(-\beta R)$, the geometric loss $G(\lambda_i) = 1 - \exp(-[2a^2]/[\omega(R)^2])$, and receiver feeder loss $\alpha_{Rj}(\lambda_i) = R_{\mathrm{SM}}(\lambda_i)R_{\mathrm{DF}}(\lambda_i)T_F(\lambda_i)T_{\mathrm{FL}}(\lambda_i)$, which leads to the received power, $P_{\mathrm{rcv}}(\lambda_i) = A_{\mathrm{rcv}}I_T(0, R)\alpha_p\alpha_{Rj}(\lambda_i)G(\lambda_i)\gamma(R)$. Here, we define A_{rcv}, $R_{\mathrm{DF}}(\lambda_i)$, $T_F(\lambda_i)$, $T_{\mathrm{FL}}(\lambda_i)$, and β as the area of receiver aperture, the reflectance of the DF at λ_i, the transmission of F, the transmission of the FL, and the atmospheric attenuation factor, respectively. Assuming shot noise σ_s and thermal noise σ_T are the two dominant noise sources, the SNR of the detected signal can be estimated as SNR $\approx [(I_{\mathrm{sig}}^2)/(\sigma_s^2 + \sigma_T^2)]$. Given that the photodiode responsivity is $R_p(\lambda_i)$, in the absence of crosstalk and negligible attenuation in space ($\beta \approx 0$), the signal photocurrent can be written as

$$I_{\mathrm{sig}} \approx 2\alpha_p \mathrm{MR}_P(\lambda_i)P(\lambda_i)\alpha_{Ti}(\lambda_i)R_{\mathrm{SM}}(\lambda_i)R_{\mathrm{DF}}(\lambda_i)$$
$$\times\ T_F(\lambda_i)T_{\mathrm{FL}}(\lambda_i)\left(1 - \exp\left(-\frac{2a^2}{\omega(R)^2}\right)\right).$$

The above-mentioned relations assume negligible crosstalk generated by the optical duplexer. As a matter of fact, at the duplexer, an incident beam splits into three major beams: 1) reflected beam; 2) transmitted beam; and 3) crosstalk component (C_T, the fraction of transmit power that goes to the receiver). In our experiment, we measure the crosstalk power generated by the COTS beam splitter and DF with an 808 nm laser source. The anti-reflective (AR) coated nonpolarizing beam splitter (700–1000 nm) has a split ratio of 50:50. With the incident optical power, $P_i = 10.4$ mW, the measured crosstalk power of the beam splitter is 12.4μ W, that is, $C_T > 0.1\%$. In such a system, a 500 mW transmit power generates $C_T > 0.5$ mW which is deleterious for long range, extremely power limited CubeSat communication systems. On the contrary, the measured C_T of an example DF is about 4 nW for P_i=10.4 mW. Therefore, C_T of a DF-based duplexer is about -65 dB, whereas C_T of a BS-based duplexer is around -30 dB. Therefore, the DF-based WSOT design as described above can increase the receiver's sensitivity by suppressing the crosstalk components. Additionally, the careful optical design as shown in Fig. 5 eliminates back reflection from the optics surfaces. We also study the mechanical feasibility of the WSOT system in the CubeSat platform through Zemax optical simulation. The example optical design is given in Fig. 6. Fig. 6 includes a beam sampler (S) that samples a fraction of the received beam and focuses on the quadrant detector (QD) to generate the feedback signal for SM. Fig. 6 shows the dimensions of the optics and the required spacings. The scanning mirror dimension is taken from a manufacturer's specs.

It is discernible from Fig. 6 that up to 5 WSOT optical units can be incorporated into about 1.5U volume ($1U \approx$ 10 cm$\times$10 cm$\times$10 cm) to achieve about 360°. Considering the electronics and other satellite subsystems, the entire CubeSat can be built in a 3U platform. The performance analyses presented in this study are based on the available power and volume of a 3U CubeSat. A larger platform (e.g., 6U, 12U, etc.) increases the SWAP-C availability for the WSOT
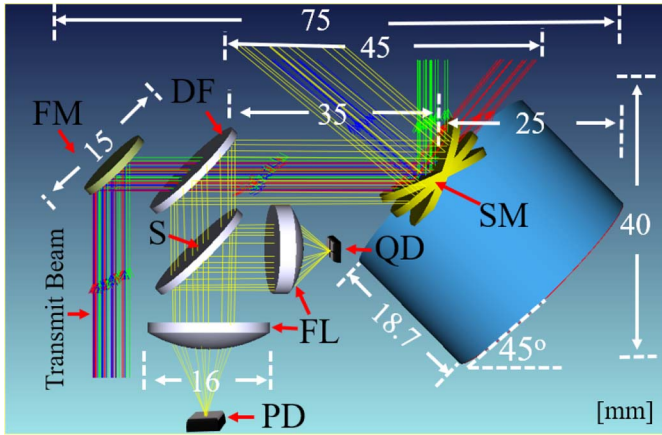
Fig. 6.   WSOT transceiver dimensions in millimeters.
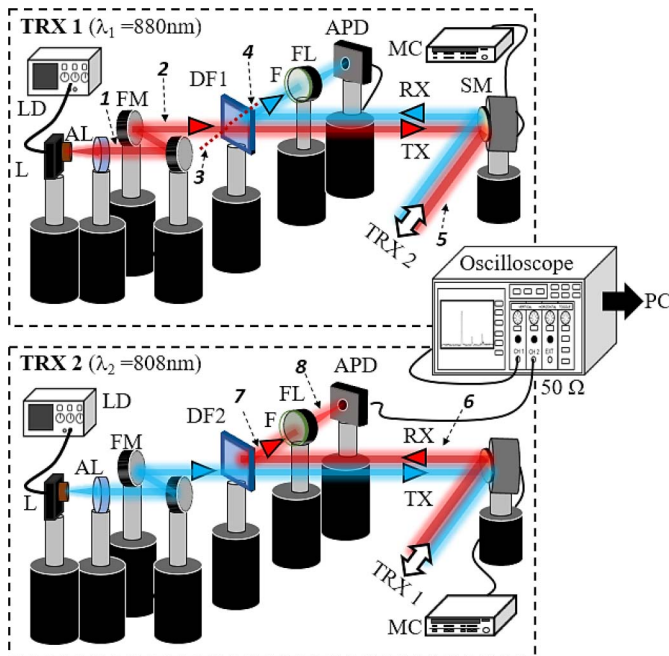
Fig. 7.   Experimental setup of the WSOT system.

payload. As a result, in larger CubeSat platform, the maximum reach and maximum attainable data rate can be extended by incorporating larger optics and higher power lasers.

IV. System Performance of the WSOT System

A. Test Bench for the WSOT System Performance Evaluation

To evaluate the performance of the WSOT system, we assemble two FlatSat models (TRX1 and TRX2) on an optical table as shown in Fig. 7 to establish a full-duplex communication. As proof of concept, we use two lasers, 808 and 880 nm, to mimic two satellites. We also incorporate an 850 nm long-pass DF and an 850 nm short-pass DF due to their availability and low cost. The lasers are then collimated using COTS AL to achieve a 10 mm transmit beam diameter. Two DFs DF1 and DF2 are integrated into the systems as duplexers. DF1 and DF2 are selected such that DF1 and DF2 allow to pass

TABLE I
Optical Power Loss of the WSOT Transceiver

Test points	Symbol	Description	Power Loss (dB)
1	L_{AL}	Collimation loss	-0.2
2	L_M	Mirror loss	-0.15
3	L_{DF}	Dichroic filter loss	-0.12
4	C_T	Crosstalk factor of DF	≈ -65
5	L_{TA1}	Scanning mirror loss (TRX1)	-0.18
6	L_{TA2}	Scanning mirror loss (TRX2)	-0.18
7	L_{DF}	Dichroic filter loss	-0.07
8	$L_F + L_{FL}$	Filter and lens lens	-0.7
	L_{OCL}	Total optical component loss	-1.6

λ_1 and λ_2, respectively, and reflect λ_2 and λ_1 to the respective receiver. Moreover, 15 mm beam SMs are also incorporated in the FlatSat models of the WSOT system. The power loss is measured at 880 nm that is transmitted by the TRX1. The receiver is fabricated using commercially available 1.00 mm Silicon APD with responsivity $R_p = 0.5$ ($M = 1$), dark current $I_D = 2\,nA$ (max), excess noise figure $F_A = 0.3$ ($\lambda = 800$ nm), and cutoff frequency, $f_c = 600$ MHz. The APD is biased at 130 V to achieve a gain (M) of about 100. A narrow band-pass filter (F) is incorporated with the FL in each receiver to reduce the ambient noise. The APD is terminated at a 2.0-GHz digital oscilloscope with a 50 Ω termination resistor. The average optical power is measured at each measurement point $i = [1, 8]$ as shown in Fig. 7 to analyze the power loss and the performance of the WSOT system. The total optical power loss L_{OL} depends on the communication distance R, optical component loss L_{OCL}, pointing loss L_{PL}, divergence angle of the transmit beam δ, and limited receiver aperture radius a and in dB scale can be expressed as

$$L_{OL}(R, a, \delta) = L_{OCL} + 10 \log\left(\frac{a^2}{R^2 + \tan^2\delta}\right) + L_{PL}. \quad (1)$$

We experimentally measure the total optical component loss of an RX-TX chain L_{OCL} of the WSOT. The measured optical power loss at different measurement points of the WSOT transceiver is summarized in Table I. L_{OCL} of the WSOT system is about 1.6 dB as shown in Table I. The measured crosstalk factor of the DF, C_T is about -65 dB. The required pointing accuracy to keep the optical throughput loss of less than 3 dB of the intersatellite optical communication can be approximated as $\epsilon \approx (\lambda/40\omega_o)$. The state-of-the-art onboard sensors have an angular resolution in the order of about 1 μrad and therefore, the required pointing accuracy can be obtained using currently accessible technologies [4], [22]. As considered in many literature (e.g., [4] and [23]), a 3 dB pointing loss, i.e., $L_{PL} = 3$ dB is considered in the link-loss calculation. The total optical power loss of the WSOT system with a 15-mm TA is presented in Fig. 8. For instance, it can be seen from Fig. 8 that 13 mm and 7.0 mm initial transmit beams experience about 60 dB optical power loss at a distance of 100 and 40 km, respectively. It is obvious from Fig. 8 that a larger transmit beam size (ω_o) experiences smaller optical loss as predicted from (1). Therefore, longer communication is achievable with a larger initial beam size. Five commercially available collimators (3, 5.5, 7, 10, and 13 mm)
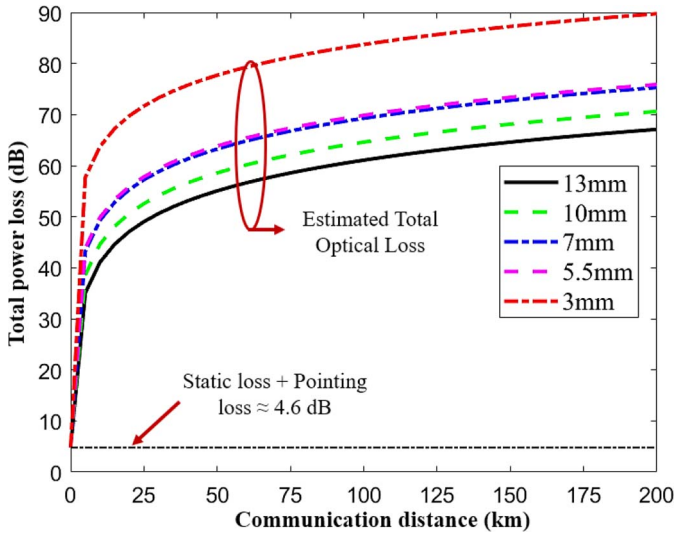
Fig. 8. Total optical loss of a WSOT system.

Fig. 9. Linear approximation of the total optical power loss for different transmit beam sizes.

TABLE II
BEAM SIZE (DIAMETER) AND HALF DIVERGENCE ANGLE

Beam size (mm)	Divergence Angle (Deg)	Beam size (mm)	Divergence Angle (Deg)
2.1	0.053	7.0	0.0072
3.0	0.038	10.0	0.0042
3.6	0.016	13.0	0.0028
4.5	0.0086	15.8	0.0025
5.5	0.0077	16.5	0.0023

are considered for the power loss calculation. In our analysis, transmitter beam size and corresponding divergence data are incorporated from commercially available optical collimators [24]–[26]. Therefore, the nonideal effects of the optics inside the collimators are considered in the Zemax simulation. The relevant transmitter beam size (diameter) and half divergence angle data are summarized in Table II.

The total power-loss-distance relation as in (1) is nonlinear. However, from the link designers' perspective, it is often convenient to quantify power loss in a linear scale, e.g., dB/km. It is observed that in long-distance communication ($R \geq 100$ km), the total power loss with respect to the distance can be approximated with a linear model. That is, total optical loss at a distance R (in km) can be approximated as $L_{\mathrm{OL}}(\mathrm{est.}) = L_o + m \times (R - 100)$ and $R \geq 100$ km. Here, L_o and m are the total power loss at 100 km and the slope of the linear fitted curve, respectively. The sample linear least square fit (LLSF) on the estimated total power-loss curve is shown in Fig. 9. Interestingly, the slope of the linear fit is independent of the initial beam sizes and divergence angle. This is evident from the parallel fitted lines in Fig. 9. For instance, it can be noted that the linear fits of the optical power loss of all initial beam sizes, e.g., 13, 10, 7 mm, etc., have the same slope m. The approximated distance-dependent incremental power loss (slope of the fitted curve, m) is 0.032 dB/km.

It is also notable that due to the small receiver aperture ($a << R$), the slope of the linear fit is also independent of the receiver aperture. The linear fitted line of the power loss
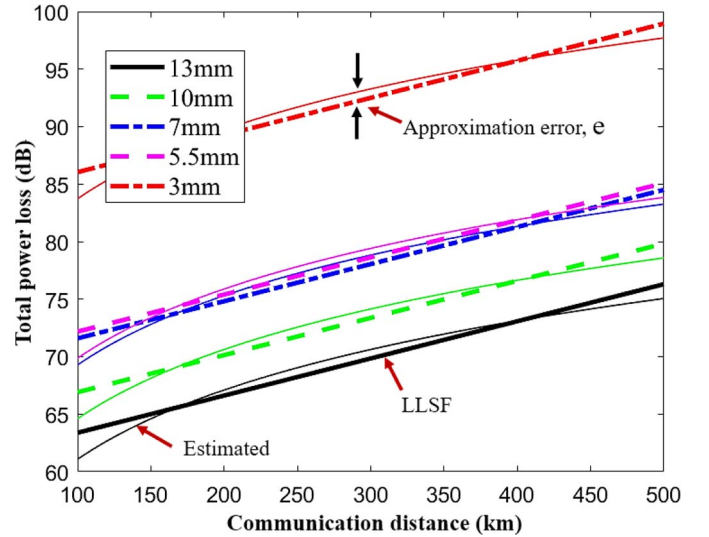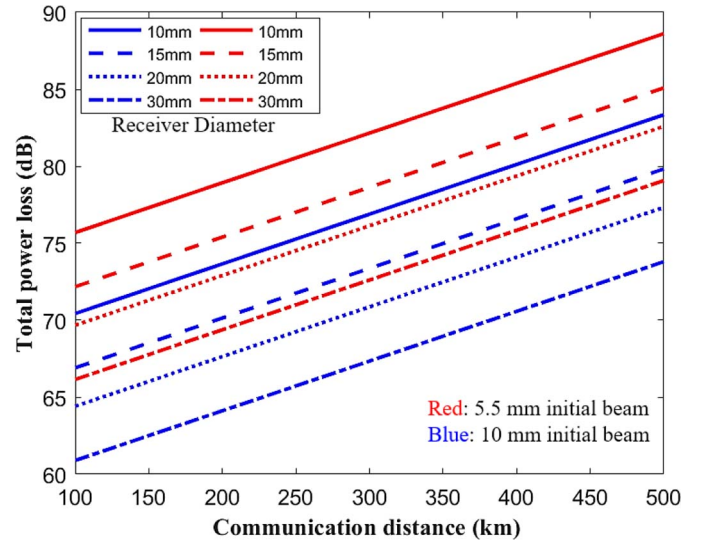
Fig. 10. Total power-loss estimation for different receiver sizes.

considering four different receiver apertures (10, 15, 20, and 30 mm) are shown in Fig. 10. Two initial beam sizes (5.5 and 10 mm) are considered in this analysis for the comparison purpose. It is evident that all fitted lines have the same m regardless of the initial beam size and the receiver dimension. The constant term, L_o of the LLSF fits for different initial beam size and different receiver diameters are summarized in Table III. The parameters L_o and m can produce a close estimation of the total power loss of the WSOT system with different initial beam sizes and receiver aperture sizes. For example, given that a WSOT system is designed with a 10-mm initial beam size and a 15 mm receiver aperture, the total optical power loss of a 200-km free-space link can be estimated as $L_{\mathrm{OL}}(\mathrm{est.}) = 66.9 + 0.032 \times (200 - 100) = 70$ dB. That is close to 70.6 dB, the value estimated from (1) and shown in Fig. 8. Furthermore, we calculate the RMS error between actual estimation and linear approximation to be $e_{\mathrm{rms}} = 0.78$ dB. The maximum error and standard deviation

TABLE III
PARAMETERS OF THE LINEAR FIT MODEL, L_o (dB)

Receiver size(mm)	10.0	15.0	20.0	30.0
Beam size(mm)				
3.0	89.6	86.1	83.5	80.1
5.5	75.7	72.2	69.7	66.2
7.0	75.1	71.6	69.0	65.6
10.0	70.4	66.9	64.4	60.8
13.0	66.9	63.38	60.9	57.4
slope of the linear fit,m= 0.032 dB/km				
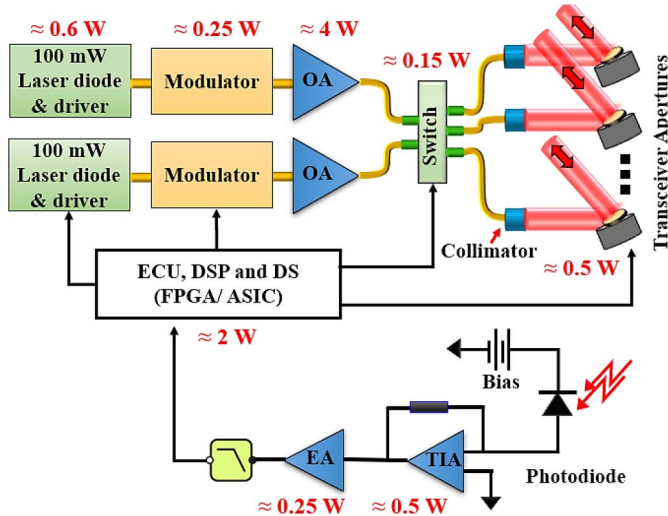
Fig. 11. Power consumption estimation of a WSOT system.

are calculated as 2.3 and 0.78 dB, respectively, for all initial beam width and receiver size combinations. This error calculation is based on the curve fitting applicable for 100 km $\leq R \leq$ 500 km.

B. Power Budget Estimation

We estimate the power consumption of the major active components of the given WSOT system. Fig. 11 shows an example of a link design that includes major electrical and optical components to establish a WSOT system. Here, we assume the wall-plug efficiency of the laser and optical amplifier (OA) are 12.5% and 16%, respectively, and average optical output is 500 mW to generate 1 W peak power considering 50% duty cycle. Also, based on different manufacturer specs, we assume the COTS TIA and electrical amplifier (EA) consume 0.5 and 0.25 W, respectively. Moreover, the electrical control unit (ECU), basic digital signal processing (DSP), and DS can be achieved with conventional FPGAs or ASICs that consume less than 2 W average power. Hence, one TX-RX has a wall-plug efficiency of about 8%. Therefore, with this example system, two links (one point to point and one relaying) can be operated simultaneously with less than 15 W power consumption. The wall-plug efficiency of the WSOT system can be further improved by using highly efficient OA and laser diodes, etc. Given that the state-of-the-art solar panels such as eHawk can generate 72 W optical power [12], a WSOT payload will consume less than 20% of the total generated
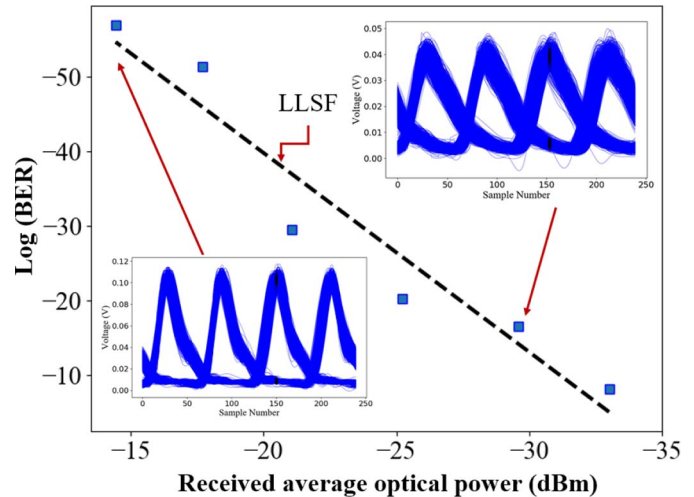
Fig. 12. BER versus received average optical power for a 200-MHz signal (sampled at 2 GS/s).

power. Since lasers are the most power-hungry components, these results are expected.

C. Data Communication Performance Test

The two FlatSat models of WSOT architectures shown in Fig. 7 are also used to test the data communication and to characterize the communication range and BER. Due to the immobility of the preliminary model, a variable free-space attenuator is placed in the optical path between two FlatSats to mimic the power loss due to different distances as estimated in Fig. 8. To estimate the BER performance, we use 200 MHz and 400 MHz square wave signals with 50% duty cycle. It is known that for a given data rate, the NRZ ON–OFF keying (OOK) modulation requires only half of the baseband bandwidth. Therefore, 200 MHz and 400 MHz signal resemble approximately 400 Mb/s and 800 Mb/s data rates, respectively. A conservative BER estimation approach based on the Gaussian statistical analysis is performed on the received signal where BER is defined as BER $= (1/2)\text{erfc}(Q/\sqrt{2})$ and quality factor, $Q = [(I_1 - I_0)/(\sigma_1 + \sigma_0)]$ [15]. I_1 and I_0 are the average received signal and σ_1 and σ_0 are the standard deviations corresponding to 1 and 0 bit, respectively. To characterize the system, the received signal (voltage) from the APD is captured by a 2 GHz oscilloscope. The captured data are then analyzed in MATLAB and Python. We create a histogram of a large number of signal segments (close to 12,000) for a credible statistical BER analysis. The BER versus received average optical power profile for 200 and 400 MHz signal are given in Figs. 12 and 13, respectively, considering NRZ-OOK modulation. The eye diagrams at different received power are given as insets. The signals are sampled at 2 GS/s. It can be seen from the figures that the minimum received power to maintain a BER $\leq 10^{-4}$ for 200 and 400 MHz signals are measured to be $S_{200} = -33$ dBm and $S_{400} = -28.5$ dBm, respectively. Note that in this analysis, the system is characterized without incorporating any TIA and RF amplifiers. The BER estimation shown in Figs. 12 and 13 is the conservative (worst case) performance of the WSOT system.
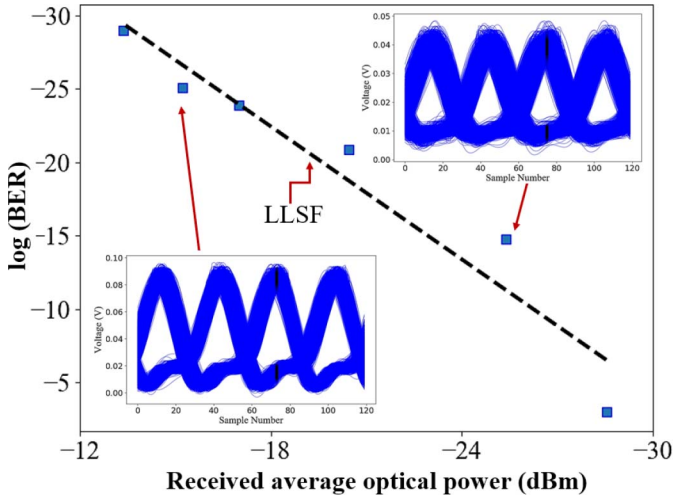
Fig. 13. BER versus received average optical power for a 400-MHz signal (sampled at 2 GS/s).

Fig. 14. Communication range estimation for 400-Mb/s WSOT system.

Fig. 15. Communication range estimation for the 800-Mb/s WSOT system.

The receiver sensitivity and estimate maximum achievable communication distance can be estimated from the above-mentioned BER analysis. Given the above-mentioned WSOT transceiver sensitivity, for a given transmit power $P(\lambda)$ and BER requirement, the maximum achievable communication distance $R_{\max}$ can be estimated by $P(\lambda) = S_k - L_{OL}(R_{\max}, a, \delta)$. Here, L_{OL} is a $-$ve quantity and the subscript $k \in \{200, 400\}$ denotes the 200 and 400 MHz signals, respectively. In order to provide readers with a better understanding of the WSOT system's scalability and to compare the performances, we study the achievable distance for four different receiver diameters, i.e., $D_R = 2a = \{10 \text{ mm}, 15 \text{ mm}, 20 \text{ mm}, 30 \text{ mm}\}$ and two signal peak powers, $P_{\text{peak}} = \{500 \text{ mW}, 1 \text{ W}\}$. For a given average power (P_{AVG}), infinite extinction ratio, and duty cycle (D_C), the theoretical attainable peak power (P_{peak}) of a laser can be estimated as $P_{\text{peak}} > P_{\text{AVG}}/D_C$. For instance, a laser operating at a 5% duty cycle and a 0.5 W average power can generate pulses with more than 10 W peak power. Up to date, several laser technologies have been demonstrated that can provide several Watts to kilo Watts of peak power [3], [27], [28]. Moreover, the received power is intertwined with the transmit beam width $\omega_{\circ}$ and therefore, in the simulation, five selected COTS collimators of beam diameters $D_T = 2\omega_{\circ} = \{13 \text{ mm}, 10 \text{ mm}, 7 \text{ mm}, 5.5 \text{ mm}, 3 \text{ mm}\}$ are incorporated from Table II. The achievable communication distance with $BER \leq 10^{-4}$ is shown in Figs. 14 and 15 for 200 and 400 MHz signals, respectively, for different D_R and P_{peak}. It can be seen from Fig. 14(a) that a 400-Mb/s data rate is achievable up to 88 km with $D_T = 13$ mm, $P_{\text{peak}} = 500$ mW, and $D_R = 15$ mm. For the same D_R and D_T, $R_{\max}$ exceeds 125 km when $P_{\text{peak}} = 1$ W as can be seen from Fig. 14(b). Furthermore, with the same system, i.e., $D_R = 15$ mm, $D_T = 13$ mm, and an 800 Mb/s (400 MHz signal) data rate can be achievable up to a distance of 53 and 80 km with 500 mW and 1 W peak power, respectively, as shown in Fig. 15. A larger transceiver aperture can achieve longer communication distance with the above-mentioned transmit power levels. For
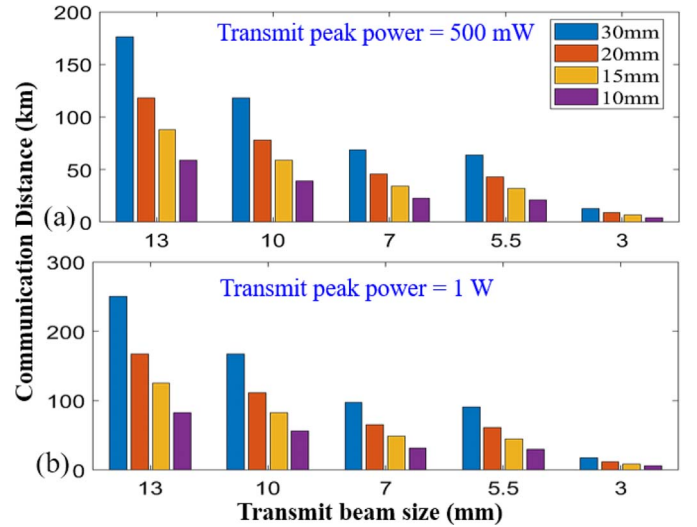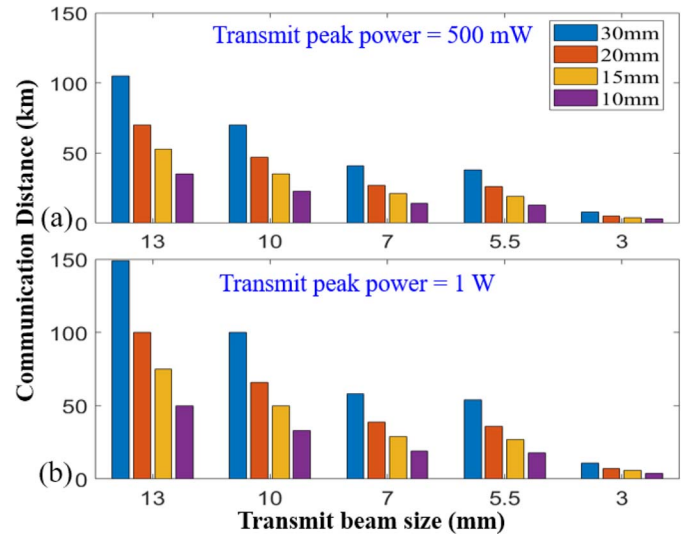
instance, it can be seen from Fig. 15(b) that an 800 Mb/s data rate is achievable up to 150 km communication distance with $P_T = 1$ W, $D_R = 30$ mm, and $D_T = 13$ mm. In our experiment, the output of the APD is terminated with a 50 Ω resistor. The proof-of-concept receiver under test does not include TIA and baseband amplifiers. In addition, a Gaussian statistical computation of the BER is adopted in the above-mentioned analysis. Therefore, the estimated link parameters (e.g., receiver sensitivity, communication distances, etc.) are the worst case scenario estimation of the WSOT link. The performance of the system can be improved further by the advanced receiver circuit design, error correction coding, and optics optimization.

V. CONCLUSION

In this article, we introduced an omnidirectional CubeSat optical crosslink concept based on WSOT. The WSOT-based optical antenna can achieve a 360° FOR that is capable of

one-to-many high-speed data communications. The optical transceiver is designed in Zemax and the performance metrics, such as receiver sensitivity, transceiver power loss, etc., are experimentally measured in the lab environment. The WSOT can achieve a data rate higher than 400 Mb/s. The expected achievable communication distance is estimated for different transmit power, transmitter aperture size, and receiver dimensions. The omnidirectional optical antenna is realizable in a 3U CubeSat dimension and expected to consume less than 15 W electrical power.

ACKNOWLEDGMENT

REFERENCES

[1] J. E. Velazco *et al.*, "Inter-satellite omnidirectional optical communicator for remote sensing," in *Proc. CubeSats NanoSats Remote Sens. II*, vol. 10769, 2018, pp. 157–162. [Online]. Available: https://doi.org/10.1117/12.2322367

[2] R. Morgan and K. Cahoy, "Nanosatellite lasercom system," in *Proc. 31st Annu. AIAA/USU Conf. Small Satellites*, 2017, pp. 1–32.

[3] R. W. Kingsbury, "Optical communications for small satellites," Ph.D. dissertation, Dept. Aeronaut. Astronaut., Massachusetts Inst. Technol., Cambridge, MA, USA, 2015.

[4] J. Kaufmann and V. Chan, "Coherent optical intersatellite crosslink systems," in *Proc. 21st Century Mil. Commun. (MILCOM)*, vol. 2, Oct. 1988, pp. 533–540.

[5] D. M. Boroson *et al.*, "Overview and results of the lunar laser communication demonstration," in *Proc. Free Space Laser Commun. Atmos. Propag. XXVI*, vol. 8971, Mar. 2014, Art. no. 89710S.

[6] A. Carrasco-Casado *et al.*, "LEO-to-ground optical communications using SOTA (small optical transponder)—Payload verification results and experiments on space quantum communications," *Acta Astronautica*, vol. 139, pp. 377–384, Oct. 2017.

[7] C. Fuchs and C. Schmidt, "Update on DLR's OSIRIS program," in *Proc. Int. Conf. Space Opt. (ICSO)*, vol. 11180, Jul. 2019, Art. no. 111800I.

[8] T. Tanaka, Y. Kawamura, and T. Tanaka, "Development and operations of nano-satellite FITSAT-1 (NIWAKA)," *Acta Astronautica*, vol. 107, pp. 112–129, Feb. 2015.

[9] T. S. Rose *et al.*, "Optical communications downlink from a 1.5u Cubesat: OCSD program," in *Proc. Int. Conf. Space Opt. (ICSO)*, vol. 11180, Jul. 2019, Art. no. 111800J.

[10] S. W Janson, "Cubesat-scale laser communications," in *Proc. Nat. Space Symp.*, 2015, pp. 1–11.

[11] K. Cahoy *et al.*, "The CubeSat laser infrared crosslinK mission (CLICK)," in *Proc. Int. Conf. Space Opt. (ICSO)*, vol. 11180, Jul. 2019, pp. 358–369.

[12] J. E. Velazco *et al.*, "High data rate inter-satellite omnidirectional optical communicator," in *Proc. 32nd Annu. AIAA/USU Conf. Small Satellites*, 2018, p. 18.

[13] I. U. Zaman, A. W. Janzen, R. Torun, J. E. Velazco, and O. Boyraz, "Design tradeoffs and challenges of omnidirectional optical antenna for high speed, long range inter CubeSat data communication," in *Proc. Small Satellite Conf. Delivering Mission Success*, Aug. 2018, p. 18.

[14] I. U. Zaman, A. W. Janzen, R. Torun, M. Peng, J. E. Velazco, and O. Boyraz, "Omnidirectional optical transceiver design techniques for multi-frequency full duplex CubeSat data communication," in *Proc. SPIE Opt. Photon. CubeSats NanoSats Remote Sens. II*, Aug. 2018, Art. no. 1076942.

[15] G. P. Agrawal, *Fiber-Optic Communication Systems*. New York, NY, USA: Wiley, 2010, pp. 162–167.

[16] M. Technologies. (2017). *Mirrorcle Technologies MEMS Mirrors—Technical Overview*. [Online]. Available: https://www.semanticscholar.org/paper/Mirrorcle-Technologies-MEMS-Mirrors-%E2%80%93-Technical/d131a1576787ffa47fbd035881ec3780cf1a09b4

[17] Optotune. *Dual Axis VCM With Position Feedback 2D Beam Steering*. Accessed: Jun. 7, 2019. [Online]. Available: https://www.optotune.com/contact/49-products/beam-steering

[18] L. Broman, "Non-imaging solar concentrators with flat mirrors," in *Proc. Int. Conf. Nonimag. Concentrators*, vol. 441, Jan. 1984, pp. 102–110.

[19] H. Ries and A. Rabl, "Edge-ray principle of nonimaging optics," *J. Opt. Soc. America A*, vol. 11, no. 10, pp. 2627–2632, Oct. 1994.

[20] J. C. Miñano and J. C. González, "New method of design of nonimaging concentrators," *Appl. Opt.*, vol. 31, no. 16, pp. 3051–3060, Jun. 1992.

[21] I. U. Zaman, J. E. Velazco, and O. Boyraz, "Wavelength selective optical system for CubeSat crosslink," in *Proc. Laser Commun. Small Satellites*, Oct. 2019, p. 4.

[22] M. Toyoshima, "Trends in satellite communications and the role of optical free-space communications [Invited]," *J. Opt. Netw.*, vol. 4, no. 6, pp. 300–311, Jun. 2005.

[23] H. Kaushal and G. Kaddoum, "Optical communication in space: Challenges and mitigation techniques," *IEEE Commun. Surveys Tuts.*, vol. 19, no. 1, pp. 57–96, 1st Quart., 2017.

[24] Microlaser, Inc. *Adjustable Fiber Collimators*. Accessed: Aug. 4, 2019. [Online]. Available: http://www.microlaser.com/FiberOptic/Fiber Collimators.html

[25] Thorlabs. *Collimation/Coupling*. Accessed: Apr. 21, 2019. [Online]. Available: https://www.thorlabs.com/navigation.cfm?guide_id=27

[26] *Fiber Components: Large-Beam Fiber Collimators*. Accessed: Sep. 28, 2019. [Online]. Available: http://www.princetel.com/fc_clx.asp

[27] A. S. Mayer, C. R. Phillips, and U. Keller, "Watt-level 10-gigahertz solid-state laser enabled by self-defocusing nonlinearities in an aperiodically poled crystal," *Nat. Commun.*, vol. 8, no. 1, pp. 1–8, Nov. 2017.

[28] F. R. Ahmad and F. Rana, "Passively mode-locked high-power (210 mW) semiconductor lasers at 1.55-μm wavelength," *IEEE Photon. Technol. Lett.*, vol. 20, no. 3, pp. 190–192, Feb. 2008.